AD-A092 317 CALIFORNIA UNIV SAN DIEGO LA JOLLA DEPT OF CHEMISTRY F/G 7/4
MOLECULAR DYNAMICS AND SPECTRA: I. DIATOMIC ROTATION AND VIBRAT--ETC(U)
NOV 80 K R WILSON, P H BERENS N00014-78-C-0325
UNCLASSIFIED TR-2 NL

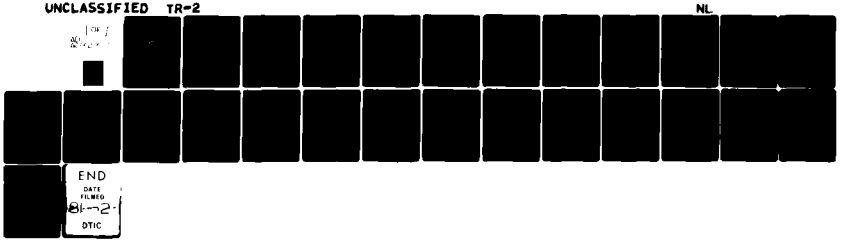

END
DATE FILMED
8-2
DTIC

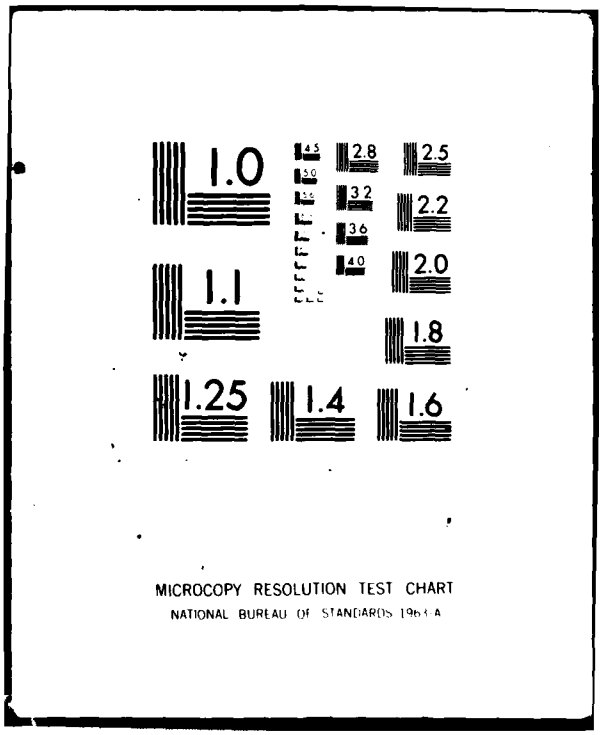
1.0
1.1
1.25
1.4
1.6
1.8
2.0
2.2
2.5
2.8
3.2
3.6
4.0
MICROCOPY RESOLUTION TEST CHART
NATIONAL BUREAU OF STANDARDS 1963-A

SECURITY CLASSIFICATION OF THIS PAGE (When Data Entered)

REPORT DOCUMENTATION PAGE

READ INSTRUCTIONS BEFORE COMPLETING FORM

1. REPORT NUMBER	2. GOVT ACCESSION NO.	3. RECIPIENT'S CATALOG NUMBER
TR-2	AD-A092317	

4. TITLE (and Subtitle)
MOLECULAR DYNAMICS AND SPECTRA: I. DIATOMIC ROTATION AND VIBRATION

5. TYPE OF REPORT & PERIOD COVERED
Technical Report

6. PERFORMING ORG. REPORT NUMBER

7. AUTHOR(s)
Kent R. Wilson
Peter H. Berens

8. CONTRACT OR GRANT NUMBER(s)
ONR-N00014-78-C-0325

9. PERFORMING ORGANIZATION NAME AND ADDRESS
Department of Chemistry
University of California, San Diego
La Jolla, CA 92093

10. PROGRAM ELEMENT, PROJECT, TASK AREA & WORK UNIT NUMBERS

11. CONTROLLING OFFICE NAME AND ADDRESS
Office of Naval Research
Arlington, VA 22217

12. REPORT DATE
November 1980

13. NUMBER OF PAGES
22

14. MONITORING AGENCY NAME & ADDRESS (if different from Controlling Office)

15. SECURITY CLASS. (of this report)
Unclassified

15a. DECLASSIFICATION/DOWNGRADING SCHEDULE

16. DISTRIBUTION STATEMENT (of this Report)
This document has been approved for public release and sale; its distribution is unlimited.

17. DISTRIBUTION STATEMENT (of the abstract entered in Block 20, if different from Report)

18. SUPPLEMENTARY NOTES
This document has been submitted to the Journal of Chemical Physics for publication.

19. KEY WORDS (Continue on reverse side if necessary and identify by block number)
molecular dynamics
diatomic rotation
diatomic vibration
vibrational spectra
computer simulation

20. ABSTRACT (Continue on reverse side if necessary and identify by block number)
The pure rotational and vibrational-rotational absorption bands for a diatomic are calculated directly from classical molecular dynamics, classical linear response theory and classical statistical mechanical ensemble averaging with the use of simple quantum corrections. The experimental spectral band intensities and contours are well reproduced for CO from dilute gas phase through solution in compressed Ar to solution in liquid Ar by these "Newtonian" classical spectral calculations. The typical evolution seen in vibrational spectra from multiple-peaked gas phase bands to single-peaked solution bands is observed.

DD FORM 1 JAN 73 1473 EDITION OF 1 NOV 65 IS OBSOLETE
S/N 0102-LF-014-6601

SECURITY CLASSIFICATION OF THIS PAGE (When Data Entered)

OVER

Block 20 (continued)

The "Newtonian" gas phase calculations also match quantum and correspondence principle classical spectral calculations. This molecular dynamic approach may be applied to compute the spectra of complex molecules or of liquids for which a normal mode analysis may be impractical, and may also be extended to non-equilibrium systems, for example to compute transient vibrational spectra during chemical reactions.

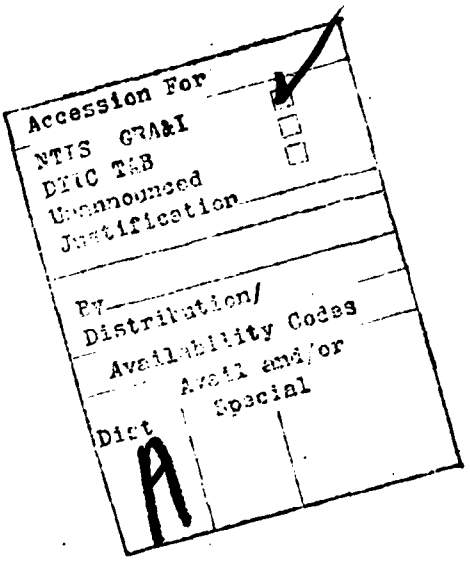

OFFICE OF NAVAL RESEARCH

Contract N00014-78 C-0325

TECHNICAL REPORT NO. 2

MOLECULAR DYNAMICS AND SPECTRA:

I. DIATOMIC ROTATION AND VIBRATION

by

Peter H. Berens and Kent R. Wilson

Submitted for Publication

to

The Journal of Chemical Physics

University of California, San Diego

Department of Chemistry

La Jolla, CA 92093

October 31, 1980

MOLECULAR DYNAMICS AND SPECTRA: I. DIATOMIC ROTATION AND VIBRATION

Peter H. Berens and Kent R. Wilson

Department of Chemistry
University of California, San Diego
La Jolla, California 92093

I. INTRODUCTION

Since one can quite easily and accurately compute the rotational and vibrational-rotational absorption spectra of diatomic molecules directly from quantum mechanics, it would at first glance seem useless, even quixotic, to try to approximate these spectra by means of a much more laborious classical technique. The justification for such an exercise is that this classical approach may be extended to systems in which a quantum approach is as yet impractical. For example, one may compute the infrared spectra for systems involving many atoms, such as large molecules, clusters or liquids, in which a normal mode analysis may not be feasible.[1] In addition, one can extend the approach to explicitly time dependent problems such as the computation of the transient vibrational spectra one might hope to measure during the course of a chemical reaction.[1-3] It is thus useful to test this approach with a simple molecular system for which the results can be rigorously tested both against accurate quantum calculations and against experimental measurements.

In Fig. 1 we see the rotational and fundamental vibrational-rotational absorption bands of CO which we will use for our test of the ability of classical mechanics to reproduce quantum reality in the form of rotational and vibrational spectra. The shapes of vibrational spectra are a sensitive reflection of both inter- and intra-molecular motion[4] and can thus in principle supply a method for discovering the microscopic trajectories responsible for chemical processes in solution.

II. THEORETICAL TECHNIQUES

The theoretical approach consists of five steps.[1] First, classical mechanics is used to compute the atomic trajectories for the system of interest from a set of initial atomic coordinates and momenta and a given potential surface. Second, a time-varying dipole moment vector (for infrared spectra) or a time-varying polarizability matrix (for Raman spectra) for the entire system is calculated from the trajectories. Third, linear response theory[4-6] is used to derive an infrared (or Raman) spectrum "specific" to the chosen initial coordinates and momenta from the power spectrum of the dipole moment (or polarizability) time histories. Fourth, the "specific" spectra are averaged over the ensemble of initial coordinates and momenta which is appropriate to the experimental conditions of interest (*e.g.* a particular temperature and pressure). Fifth, quantum corrections are applied where necessary to converge toward quantum reality.

By these five steps, surprisingly accurate infrared and Raman spectra may be derived from three functions of atomic coordinates: potential energy, dipole moment vector and polarizability matrix. We will illustrate here the electric dipole (microwave and infrared absorption and emission) case, and leave the details of Raman scattering for another paper.

A. Molecular Dynamics and Classical Trajectories

Our first step is to choose a set of initial coordinates and momenta for the collection of N atoms from an ensemble of possibilities representative of the system of interest, for example a system at a particular pressure and temperature. We make this choice purely classically although Marcus and co-workers have shown[7] how one might also make such choices semiclassically. The second step is to compute the classical trajectories $\mathbf{r}_1(t), \ldots, \mathbf{r}_N(t)$ describing the atomic motions by integrating Newton's Second Law

$$-\frac{\partial V}{\partial \mathbf{r}_i} = \mathbf{F}_i = m_i \frac{d^2\mathbf{r}_i}{dt^2}, \quad i = 1, \ldots, N \tag{1}$$

in which $V = V(\mathbf{r}_1, \ldots, \mathbf{r}_N)$ is the potential energy of the atoms at positions $\mathbf{r}_1, \ldots, \mathbf{r}_N$, $\mathbf{F}_i = \mathbf{F}_i(\mathbf{r}_1, \ldots, \mathbf{r}_N)$ is the force on the i th atom, and m_i is the mass of the i th atom. A modified Verlet integration algorithm is used.[8,9] For the example shown below of a CO solution in Ar, minimum image periodic boundary conditions with truncated octahedral boundaries[10] are used to reduce edge effects.

B. Time History of Dipole Moment

Given the function $\boldsymbol{\mu}(\mathbf{r}_1, \ldots, \mathbf{r}_N)$, which describes the dipole moment of the system as a function of the atomic positions, we can use the trajectories of the atoms, $\mathbf{r}_1(t), \ldots, \mathbf{r}_N(t)$, to compute $\boldsymbol{\mu}(t)$, the dipole moment of the system as a function of time.

C. Linear Response and Specific Spectra

For a system at equilibrium, we can use linear response theory[4-6] to compute the infrared spectrum $\alpha(\omega)$ from the dipole moment time history, $\boldsymbol{\mu}(t)$. We can thus relate the spectrum of the fluctuations which $\boldsymbol{\mu}(t)$ naturally undergoes at equilibrium to the spectrum with which $\boldsymbol{\mu}(t)$ responds when driven by an external oscillating electric field, *i.e.* we relate the equilibrium dipole moment fluctuation spectrum to the absorption spectrum when irradiated with light.

The appropriate linear response equations are[4,6]

$$\alpha(\omega) = \frac{4\pi^2\omega[1-\exp(-\beta\hbar\omega)]}{3\hbar cn} I(\omega) \tag{2}$$

$$I(\omega) = (2\pi)^{-1} \int_{-\infty}^{\infty} dt \exp(-i\omega t) \langle \boldsymbol{\mu}(0)\cdot\boldsymbol{\mu}(t) \rangle \tag{3}$$

in which $\alpha(\omega)$ is the absorption cross section as a function of angular frequency ω, $\beta = (k_B T)^{-1}$ in which k_B is Boltzmann's constant and T the temperature, $\hbar = h/2\pi$ in which h is Planck's constant, c is the speed of light, n is the index of refraction of the medium, $I(\omega)$ is defined as the absorption lineshape and is evaluated for an isotropic medium, and $\langle \boldsymbol{\mu}(0)\cdot\boldsymbol{\mu}(t) \rangle$ is the ensemble average of the dipole moment time correlation function.

As Parseval's theorem[11] and the Wiener-Khintchine theorem [6,12] show, $I(\omega)$ may be computed in the mathematically equivalent form of the power spectrum[7]

$$I(\omega) = (2\pi)^{-1} \left[\lim_{\tau\to\infty} \frac{1}{2\tau} \sum_{j=x,y,z} \left| \int_{-\tau}^{\tau} dt \exp(-i\omega t)\mu_j(t) \right|^2 \right] \tag{4}$$

allowing the use of fast Fourier techniques. Considerable care must be used to properly apply spectral estimation theory, windowing and windowing corrections,[11,13] in both the correlation and power spectra methods to avoid distorting the spectra as a result of the use of finite time histories. Particular care must be taken if band wings are to be correct or if small bands are to be seen in the presence of large ones. We use a four term −74 db Blackman-Harris window,[13] which allows the correction to be applied as a simple frequency-space convolution of the Fourier transform of the dipole moment time histories with the Fourier transform of the window function. This is done before computing the power spectrum. The windowed power

spectrum is multiplied by the inverse of the sum of the squares of the windowing function which, by Parseval's theorem,[11] can be evaluated either in time (windowing function) or frequency (Fourier transform of windowing function). This simple scaling factor corrects the spectral band areas for the scaling effect of the windowing and is correct because of the loss of phase coherence due to the ensemble averaging. The windowing and the area scaling correction can be combined into a convolution of the Fourier transform of the dipole moment time history with the discrete function $f_k = (-0.00170, 0.08725, -0.46174, 0.74724, -0.46174, 0.08725, -0.00170)$ for $k = -3, \ldots, 0, \ldots, +3$ before taking the square of the absolute value in computing the power spectrum.

D. Ensemble Averaging

The specific spectrum computed from a single time history is the spectrum of a particular very small sample for a particular very short time period. To compare to an experimental spectrum, an ensemble average must be made over a distribution of specific spectra corresponding to the experimental conditions. For example, to compare with a spectrum taken at temperature T one can choose a reasonable initial guess for the positions $\mathbf{r}_1(0), \ldots, \mathbf{r}_N(0)$ of the atoms, and choose the velocities $\dot{\mathbf{r}}_1(0), \ldots, \dot{\mathbf{r}}_N(0)$ randomly from a Maxwell-Boltzmann distribution for temperature T. After computing the trajectories $\mathbf{r}_1(t), \ldots, \mathbf{r}_N(t)$ forward in time for a suitable period to equilibrate the system (in particular to equilibrate potential and kinetic energies) one can preserve positions but change to a new set of velocities, again chosen randomly from the Maxwell-Boltzmann distribution, and then continue integrating forward in time. (Such velocity randomization is important to achieve a proper ensemble average for low density gas phase molecules for which energy and angular momentum are otherwise conserved over long periods.) Several repetitions of this process will result in a system equilibrated at the desired temperature T and randomly chosen as to velocity. The positions of the atoms may still, however, be correlated with the initial guessed positions. To sample more of configuration space we therefore use the final positions of each run as the initial guess for the next run and again repetitively randomize velocities. An alternative method would be to use the semiclassical techniques of Marcus and co-workers[7] and quantize the action variables and then perform the ensemble average over a Boltzmann population of these quantized systems.

The spectra which are derived from classical molecular dynamics, classical linear response theory, and classical statistical mechanical ensemble averaging we will call "Newtonian." They are straightforward to calculate in principle, but can be unusually demanding arithmetically. Thus for their computation we use what might be called an "instrument for theory," a network of processors (including an array processor) and generalized program package, which are described elsewhere.[1,2]

E. Quantum Corrections

In order to discover what corrections are necessary to bring our classical calculations into agreement with quantum reality, we will compare three different ways of computing the absorption spectrum: *i*) quantum mechanics without linear response theory, *ii*) correspondence principle classical mechanics without linear response theory as given by the limit of quantum mechanics as Planck's constant approaches zero, and *iii*) ordinary Newtonian classical mechanics with classical linear response theory and ensemble averaging from classical statistical mechanics.

1. Quantum solution

Quantum mechanically, we can evaluate the absorption spectrum, $\alpha(\omega)$, from $I(\omega)$ as shown in Eq. (2), without recourse to linear response theory as,[4,6]

$$I(\omega) = \sum_i \sum_f \rho_i \, |<f|\mu|i>|^2 \, \delta(\omega_{fi} - \omega) \tag{5}$$

in which we have averaged over an isotropic distribution of molecular orientations. In the above, i is an initial quantum state, f a final state, $\rho_i = \exp(-\beta E_i)/\sum_i \exp(-\beta E_i)$ is the probability for initial state i, $<f|\mu|i>$ is the electric dipole transition matrix element between states i and f, $\omega_{fi} = (E_f - E_i)/\hbar$, E_f and E_i are the energies of the final and initial states, respectively, and δ is the Dirac delta function. In the Appendix, we give the evaluation of this expression explicitly for the case of the isolated diatomic molecule and thus arrive at a quantum mechanical computation of the rotational and vibrational-rotational spectrum $\alpha(\omega)$, by inserting the resulting $I(\omega)$ into Eq. (2).

2. Correspondence principle classical solution

We can solve problems in classical mechanics in either of two very different ways. We can take the usual route of Newton's laws, or, as in this section, we can solve the problem quantum mechanically, but take the correspondence principle limit as $\hbar \to 0$. Both forms of classical mechanics are useful in bringing different viewpoints to bear on understanding the problem, and in providing checks of theoretical and computational methods. The correspondence principle approach, *i.e.* the limit of infinitesimal photons causing infinitesimal perturbations of the molecular system, gives for the classical $\hbar \to 0$ limit of Eq. (2)

$$\alpha(\omega) = \frac{4\pi^2\omega^2\beta}{3cn} \, I(\omega) \tag{6}$$

which we use with our classical molecular dynamics calculations.

However, in the correspondence principle calculations illustrated in the figures, we have taken the $\hbar \to 0$ limit by iterating each calculation of $\alpha(\omega)$ using successively lower values of $\hbar$ in Eqs. (A7-A9) of the Appendix and in Eq. (2) until the computed $\alpha(\omega)$ converges, which occurs by the time $\hbar$ has been replaced by $\sim 0.01\hbar$.

3. Evaluation of quantum corrections

Simple quantum corrections are used to bring the classically computed spectra into agreement with theoretical and experimental quantum reality. The correction to the rotational band contour will be seen to be minor and usually negligible. The vibrational-rotational contour correction, while not negligible, is relatively small and easy to apply, consisting of a frequency shift and a shape correction.

We write Eq. (2) as

$$\alpha^Q(\omega) = \frac{4\pi^2\omega[1-\exp(-\beta\hbar\omega)]}{3\hbar cn} \, I^Q(\omega) \tag{7}$$

in which the superscript Q indicates quantum. If we substitute $-\omega$ for ω, interchange the subscripts i and f in Eq. (5), and recognize that $|<f|\mu|i>|^2 = |<i|\mu|f>|^2$ and $\delta(\omega) = \delta(-\omega)$, we then find that

$$I^Q(-\omega) = \sum_i \sum_f \rho_f \, |<f|\mu|i>|^2 \, \delta(\omega_{fi} - \omega). \tag{8}$$

For a system at equilibrium, $\rho_i = \exp(\beta\hbar\omega_{fi})\rho_f$, and thus

$$\frac{I^Q(\omega)}{I^Q(-\omega)} = \exp(\beta\hbar\omega_{fi}) = \exp(\beta\hbar\omega) \, , \tag{9}$$

which is just an expression of detailed balance. Because of the δ-functions in Eqs. (5) and (8), ω can replace ω_{ji}. The correspondence principle classical limit is thus

$$\frac{I^C(\omega)}{I^C(-\omega)} = \lim_{\hbar\to 0} \frac{I^Q(\omega)}{I^Q(-\omega)} = 1 , \tag{10}$$

in which the superscript C indicates classical. Eqs. (9) and (10) can be understood as follows. The energy carried by a photon of angular frequency ω connects states in a quantum system which are $\hbar\omega$ apart and of appreciably different Boltzmann probabilities in an equilibrium system, and thus the $I^Q(\omega)$ for absorption and $I^Q(-\omega)$ for emission are related by the detailed balance factor $\exp(\beta\hbar\omega)$. In the classical correspondence limit as $\hbar\to 0$, the photon connects states of only infinitesimally different energy thus $I^C(\omega)$ for absorption and $I^C(-\omega)$ for emission become equal. Comparison of Eqs. (9) and (10) suggests that one should consider the quantum correction[5, 14, 15]

$$\frac{I^Q(\omega)}{I^C(\omega)} = \exp(\beta\hbar\omega/2) \tag{11}$$

which symmetrically and simply fulfills the requirements of both equations. The factor of $\omega/2$ inside the exponential in Eq. (11) arises because $I^Q(-\omega)$ and $I^Q(\omega)$, which are related by detailed balance, lie 2ω apart in angular frequency.

a. Rotational correction. The classical absorption cross section $\alpha^C(\omega)$ is, from Eq. (7),

$$\alpha^C(\omega) = \lim_{\hbar\to 0} \alpha^Q(\omega) = \left[\frac{4\pi^2\omega}{3cn} \lim_{\hbar\to 0} \frac{[1-\exp(-\beta\hbar\omega)]}{\hbar}\right] \left[\lim_{\hbar\to 0} I^Q(\omega)\right] \tag{12}$$

$$= \frac{4\pi^2\omega^2\beta}{3cn} I^C(\omega), \tag{13}$$

in which we define the correspondence principle, $\hbar\to 0$, classical limit of $I^Q(\omega)$ as $I^C(\omega)$.

Using Eqs. (7), (11) and (13) we have,

$$\frac{\alpha^Q(\omega)}{\alpha^C(\omega)} = \frac{\sinh(\beta\hbar\omega/2)}{\beta\hbar\omega/2} \tag{14}$$

which can be used as a quantum correction to $\alpha^C(\omega)$, the classical pure rotational band contour. Since for small x, $\sinh(x) \approx x$, the quantum correction is approximately unity for low frequencies and high temperatures, and is only 1.0096 at 100 cm^{-1} and 300 °K. Thus, in general its effect on the rotational spectrum is small and the quantum and classical pure rotational band contours are essentially the same.

b. Vibrational-rotational correction. To derive quantum corrections for the vibrational-rotational spectra, we first make the approximation of separating vibration and rotation (a separation not made in our molecular dynamics which can mix and couple translational, rotational and vibrational motions), giving for the matrix element in Eq. (5), as shown in Eq. (A4) of the Appendix,

$$\langle f|\mu|i\rangle = \langle v'J'M'|\mu|vJM\rangle \tag{15}$$

$$\approx \langle v'|\mu(R)|v\rangle \langle J'M'|\hat{\mathbf{R}}|JM\rangle \tag{16}$$

in which $\mu(R)$ is the magnitude of the dipole moment and $\hat{\mathbf{R}}$ is a unit vector along the internuclear axis. We also drop, for example in Eq. (A11), the coupling terms between vibration and rotation in the energy which gives

$$\hbar\omega_{fi} = E(v',J') - E(v,J)$$

$$\approx [E(v') - E(v)] + [E(J') - E(J)] = \hbar\omega_{v'v} + \hbar\omega_{J'J} , \tag{17}$$

where $\omega_{v'v}$ and $\omega_{J'J}$ are angular frequency differences between states v' and v and J' and J respectively. Substituting Eqs. (16) and (17) into Eq. (5) we get

$$I^Q(\omega) = \sum_{v}\sum_{v'}\sum_{J,M}\sum_{J'M'} \rho_i(v)\,\rho_i(J)\,|<v'|\mu(R)|v>\,<J'M'|\hat{\mathbf{R}}|JM>|^2 \times \delta(\omega_{v'v} + \omega_{J'J} - \omega), \tag{18}$$

in which, for a system at equilibrium,

$$\rho_i(v) = \frac{\exp[-\beta E(v)]}{\sum_v \exp[-\beta E(v)]} \tag{19}$$

and

$$\rho_i(J) = \frac{\exp[-\beta E(J)]}{\sum_J \exp[-\beta E(J)]} . \tag{20}$$

Separtation of the sums over the vibrational and rotational states gives

$$I^Q(\omega) = \left[\sum_v\sum_{v'}\rho_i(v)\,|<v'|\mu(R)|v>|^2\right]\left[\sum_{J,M}\sum_{J'M'}\rho_i(J)\,|<J'M'|\hat{\mathbf{R}}|JM>|^2\right] \times\ \delta(\omega_{v'v} + \omega_{J'J} - \omega) . \tag{21}$$

We can write this in terms of a convolution[16]

$$I^Q(\omega) = \left[\sum_v\sum_{v'}\rho_i(v)\,|<v'|\mu(R)|v>|^2\,\delta(\omega_{v'v} - \omega)\right] * \left[\sum_{J,M}\sum_{J'M'}\rho_i(J)\,|<J'M'|\hat{\mathbf{R}}|JM>|^2\,\delta(\omega_{J'J} - \omega)\right] \tag{22}$$

$$= I_V^Q(\omega)\ *\ I_R^Q(\omega), \tag{23}$$

in which the quantum absorption lineshape $I^Q(\omega)$ is seen to be a convolution of the quantum vibrational absorption lineshape $I_V^Q(\omega)$ and the quantum rotational absorption lineshape $I_R^Q(\omega)$, if vibration and rotation are separable by Eqs. (16) and (17). Therefore, in this approximation of separation of vibration and rotation, we can quantum correct the vibrational and rotational lineshapes $I_V^Q(\omega)$ and $I_R^Q(\omega)$ separately and then convolve the results.

Similarly, when vibration and rotation are separable by Eqs. (16) and (17), by applying the frequency convolution theorem[11] to Eq. (23), we can separate the dipole moment time correlation function[4,6] into a product of vibrational and rotational correlation functions[17]

$$<\boldsymbol{\mu}(0)\cdot\boldsymbol{\mu}(t)> = \int_{-\infty}^{\infty} d\omega\,\exp(i\omega t)\,I^Q(\omega) = \int_{-\infty}^{\infty} d\omega\,\exp(i\omega t)\left[I_V^Q(\omega)\ *\ I_R^Q(\omega)\right] \tag{24}$$

$$= \left[\int_{-\infty}^{\infty} d\omega\,\exp(i\omega t)\,I_V^Q(\omega)\right]\left[\int_{-\infty}^{\infty} d\omega\,\exp(i\omega t)\,I_R^Q(\omega)\right] \tag{25}$$

$$= <\boldsymbol{\mu}(0)\boldsymbol{\mu}(t)>\,<\hat{\mathbf{R}}(0)\cdot\hat{\mathbf{R}}(t)> . \tag{26}$$

Substituting Eq. (23) into Eq. (7), the quantum vibrational-rotational absorption cross section, *i.e.* spectrum, is

$$\alpha^Q(\omega) = \left[\frac{4\pi^2\omega[1-\exp(-\beta\hbar\omega)]}{3\hbar cn}\right]\left[I_V^Q(\omega)\ *\ I_R^Q(\omega)\right] \tag{27}$$

and the classical spectrum is

$$\alpha^C(\omega) = \lim_{\hbar\to 0} \alpha^Q(\omega) = \left[\frac{4\pi^2\omega}{3cn} \lim_{\hbar\to 0} \frac{1-\exp(-\beta\hbar\omega)}{\hbar}\right] \left\{\left[\lim_{\hbar\to 0} I_V^Q(\omega)\right] * \left[\lim_{\hbar\to 0} I_R^Q(\omega)\right]\right\} \tag{28}$$

$$= \left[\frac{4\pi^2\omega^2\beta}{3cn}\right] [I_V^C(\omega) * I_R^C(\omega)] . \tag{29}$$

A comparison of Eqs. (27) and (29) shows that given the classical vibrational-rotational spectrum, $\alpha^C(\omega)$, and assuming separability of vibration and rotation, we can quantum correct it to approximate the quantum band contour by the following three steps.

i) Initial factor. The ratio of the quantum and classical versions of the first factor in brackets in Eqs. (27) and (29) is

$$\frac{\frac{4\pi^2\omega}{3cn} \cdot \frac{[1-\exp(-\beta\hbar\omega)]}{\hbar}}{\frac{4\pi^2\omega^2\beta}{3cn}} = \frac{1-\exp(-\beta\hbar\omega)}{\beta\hbar\omega} , \tag{30}$$

and we multiply the classical spectrum by this factor.

ii) Vibrational lineshape. From Eqs. (22) and (23), we have

$$I_V^Q(\omega) = \sum_v \sum_{v'} \rho_i(v) \; |<v'|\mu(R)|v>|^2 \; \delta(\omega_{v'v} - \omega) . \tag{31}$$

If we evaluate $I_V^Q(\omega)$, the vibrational absorption lineshape function, using the linear dipole function approximation, $\mu(R) \approx \mu_0 + \mu_1 \Delta R$, for an equilibrium system of harmonic oscillators (see Appendix) we find[18]

$$I_V^Q(\omega) = \frac{\hbar}{2m_r\omega[1-\exp(-\beta\hbar\omega)]} \; \mu_1^2 \; \delta(\omega_o - \omega) \tag{32}$$

in which m_r is the reduced mass of the oscillator, $\omega_o = (k/m_r)^{1/2}$ and k is the force constant. Taking the correspondence principle limit of Eq. (32) yields

$$I_V^C(\omega) = \lim_{\hbar\to 0} I_V^Q(\omega) = (2m_r\beta\omega^2)^{-1} \; \mu_1^2 \; \delta(\omega_o - \omega) , \tag{33}$$

giving a quantum correction factor from Eqs. (32) and (33) of

$$\frac{I_V^Q(\omega)}{I_V^C(\omega)} = \frac{\beta\hbar\omega}{1-\exp(-\beta\hbar\omega)} . \tag{34}$$

This harmonic oscillator quantum correction factor exactly cancels out the quantum correction in Eq. (30) above. Therefore, for a harmonic oscillator with linear dipole moment function, there is no quantum correction and the quantum and classical spectra agree for pure vibration. The quantum corrections to vibration are thus due to anharmonicity in the potential and non-linearity in the dipole moment function. We will discuss only the potential anharmonicity here.

For the fundamental absorption band, the sum of all $v+1 \leftarrow v$ transitions, the dominant effect of potential anharmonicity for pure vibration is a shift in the band center to a lower frequency. That such a quantum correction is needed can be seen qualitatively as follows. For a usual high frequency vibration at room temperature, the classical oscillator is at $\sim k_B T$, near the bottom of the well in a largely harmonic region, while the quantum oscillator is transitioning largely from the zero point $v=0$ to $v=1$ levels (both at several $k_B T$) thus feeling much more of the anharmonicity.

A simple correction suffices for the $\Delta v=1$ fundamental transition treated here. We need only shift the whole band as calculated classically over to its proper quantum location, without needing to alter its shape. This can be done by computing the shift of the rotationless oscillator, involving the fictitious (v,J) transitions $(v+1,0) \leftarrow (v,0)$. We can derive this pure vibrational spectrum from Eq. (A8) in the Appendix as

$$I_V^Q(\omega) = \sum_{v=0}^{\infty} \rho(v,0)\, \mu_f^2\, [(v+1)/2\alpha]\, \delta\left[\frac{E(v+1,0) - E(v,0)}{\hbar} - \omega\right]. \tag{35}$$

We evaluate the center in angular frequency of $\alpha(\omega)$ for the vibrational band as computed from Eqs. (2) and (35), first for the quantum case and then for the classical case by reducing Planck's constant until convergence is reached. This offset between the classical and quantum rotationless band centers is then used to shift the classical vibrational-rotational band contour into its quantum corrected position.

While this procedure can be quickly carried out, there is also a rougher approximation which can be used. Classical oscillation is often so close to the bottom of the potential well that a classical vibration sees essentially only the harmonic part of the potential and thus only the ν_e term in Eq. (A11) in the Appendix is important. Quantum mechanically, if $h\nu_e$ is high enough with respect to $k_B T$, only $v=0$ will be appreciably populated, and only 1—0 vibrational transitions need be considered. Then the offset in angular frequency ω is approximately $-4\pi\nu_e x_e$, as may be computed from Eq. (A11).

iii) Rotational lineshape. Comparing Eqs. (27) and (29), and noting Eq. (11), we can quantum correct the rotational absorption lineshape function $I_R^C(\omega)$ for the vibrational-rotational band by multiplying it by $\exp[\beta\hbar(\Delta\omega)/2]$, in which $\Delta\omega$ is the frequency measured from the rotationless center of the vibrational band.[19,20] This factor can be understood by considering rotation as a mechanically and statistically separate process from vibration in which $+\Delta\omega$ is a rotational absorption from f—i and $-\Delta\omega$ a rotational emission from f—i, and the frequency difference $2\Delta\omega$ therefore separates processes for which detailed balance gives a probability ratio of $\exp[\beta\hbar(\Delta\omega)]$ at equilibrium.

Thus, the classical fundamental vibration-rotation spectrum can be quantum corrected by two easy steps. First, the spectrum is frequency shifted to take into account the effect of vibrational anharmonicity, and second, it is multiplied by $\exp[\beta\hbar(\Delta\omega)/2]$. This assumes that vibration and rotation are approximately independent, so that detailed balance may be applied separately to each. This assumption is not necessarily appropriate for condensed systems.

In Fig. 2 we show some of the effects of the various quantum corrections discussed above for the fundamental vibration-rotation absorption band of gas phase CO. First of all, the upper panel shows the quantum band contour from Eqs. (2), (5) and (A8-A18) as a solid line. The dotted line shows the classical band contour from the $\hbar$—0 limit of these equations. The dashed line shows the effect of applying the vibrational anharmonic offset quantum correction of $-22\ \text{cm}^{-1}$ at 300°K from Eq. (35) (the rougher approximation of $-4\pi\nu_e x_e$ gives[21] $-26\ \text{cm}^{-1}$). The dashed and dotted line shows the effect of applying the rotational detailed balance correction $\exp[\beta\hbar(\Delta\omega)/2]$ alone to the classical vibration-rotation band contour. The effect of applying both the vibrational offset and the rotational detailed balance corrections is shown by open circles, and is seen to match very closely the true quantum contour.

The lower panel of Fig. 2 shows the large effect of vibrational anharmonicity on the band contour. The computations are similar to those shown in the upper panel, except that CO is treated as a harmonic oscillator. The same equilibrium internuclear distance and second derivative of the potential are used as for previous case, but the third, fourth, and higher derivatives are set to zero. There is now no anharmonic offset. The solid line shows the quantum band contour, the dotted line the classical contour, and the open circles the effect of applying the rotational detailed balance correction. It should be noted for the real anharmonic CO band contour that the difference in peak intensity of the P and R branches is much more pronounced than for the harmonic case. The inability to match the P and R branch asymmetry of real spectra with harmonic oscillator - rigid rotor models has been a source of confusion. It appears from Fig. 2 that the problem has not been a quantum effect at all, but simply due to ignoring the true anharmonicity of the potential.

III. PURE ROTATIONAL SPECTRA

Fig. 3 shows the pure rotational band for gas phase CO. The upper panel shows the quantum mechanical spectrum, computed as shown in the Appendix in Eqs. (A7) and (A10-A18) by explicitly calculating the individual transitions with the usual time-dependent perturbation theory approach to compute $I(\omega)$, and then using Eq. (2) to compute $\alpha(\omega)$. The solid line shows the quantum band contour, given by broadening the individual transition lineshapes until they merge, using Eq. (A18). The CO potential used in all these calculations is Huffaker's analytical expansion,[22,23] giving, for use in the quantum and correspondence principle classical calculations, the potential derivative values at the equilibrium internuclear distance R_e of $V''(R_e)=1.92024\times10^{-3}$ J m^{-2}, $V''''(R_e)=-1.36445\times10^{-14}$ J m^{-3} and $V''''''(R_e)=8.08245\times10^{-24}$ J m^{-4}. We used[21] $R_e=1.128323\times10^{-10}$ m and reduced mass $m_r=1.13843\times10^{-26}$ kg.

The middle panel of Fig. 3 demonstrates that the classical, correspondence principle, $\hbar\rightarrow0$ limit pure rotational band contour falls almost exactly on the quantum contour. The total area of the rotational band is 1.88×10^{-22}m, close to the area of 1.94×10^{-22}m indicated by the free rigid rotor sum rule

$$\int\sigma\, d\lambda^{-1} = \frac{2\pi}{3\times10^{7}}\cdot\frac{\mu_0^2}{I}\,, \tag{36}$$

given by Buontempo *et al.*[24] Eq. (36) is given in SI units, σ is the absorption cross section, λ^{-1} the inverse wavelength, μ_0 the permanent dipole moment and I the moment of inertia.

The lower panel of Fig. 3 demonstrates that "Newtonian" classical mechanics, calculated from classical molecular dynamics as in Eq. (1), classical linear response theory as in Eqs. (4) and (6) and classical statistical mechanical averaging also agrees with quantum reality. In addition, it is seen that the calculations essentially agree with the experimental gas phase measurements of Buontempo *et al*[24] on 1.6% CO solution broadened by Ar at 17.4 atm.

Thus, for the gas-phase CO rotational band contour, *i*) quantum, *ii*) correspondence principle classical, *iii*) Newtonian classical and *iv*) experiment all agree.

IV. VIBRATIONAL-ROTATIONAL SPECTRA

Figure 4 shows the fundamental vibrational-rotational band for gas phase CO. The top panel gives the results from quantum mechanics, the total effect of all the vibrational-rotational transitions calculated from time-dependent perturbation theory as discussed in the Appendix. The quantum vibrational-rotational lines in the P and R branches are computed explicitly from the quantum transitions and then checked against accurate line position measurements.[25] The quantum band contour is produced by widening out the lines as gaussians until they merge, as calculated from Eq. (2) and Eqs. (A8-A18) in the Appendix.

The middle panel of Fig. 4 shows that the correspondence principle classical result, as calculated as the $\hbar\rightarrow0$ limit of the above quantum transition result, agrees almost exactly with the quantum result when the rotational and vibrational quantum corrections described above are applied.

The lower panel of Fig. 4 shows the Newtonian classical result, computed from classical molecular dynamics by Eq. (1), classical linear response theory, and classical ensemble averaging, and then quantum corrected in the same way as in the middle panel. Newtonian classical mechanics is seen also to agree very closely with the quantum result. In addition, as shown, the experimental results of Armstrong and Welsh[26] for CO broadened by 104 amagats of He also agree in shape (no experimental absolute intensity was given).

Thus, four approaches all give essentially the same answer: *i*) quantum mechanics (time-dependent perturbation theory), *ii*) quantum-corrected correspondence principle classical mechanics as the $\hbar\rightarrow0$ limit of quantum mechanics, *iii*) quantum-corrected Newtonian classical mechanics plus classical linear response theory and classical statistical mechanics and *iv*) experimental measurement.

In the above calculations, we used a linear averaged approximation to the dipole moment function, Eq. (A3) in the Appendix, to facilitate a more parallel comparison among the various theoretical approaches, choosing[27-29] $<\mu_0>=-0.1098$ Debye for the averaged permanent dipole moment and $<\mu_1>=3.1$ Debye/Å for the dipole moment first derivative. (1 Debye = 3.336×10^{-30} coulomb-meter.) The Newtonian approach may trivially be extended to any dipole moment function and, at the cost of some algebraic complexity, the quantum and $\hbar\to0$ classical approaches may also be extended.[27,30-32] Additional quantum corrections to the classical intensities may then be required. Given a dipole moment function, any of the theoretical approaches can be used to compute the spectral intensities for rotational and vibrational-rotational transitions more accurately than they are readily experimentally measurable.[28,29,33,34]

V. FROM GAS TO LIQUID

Having demonstrated that the quantum-corrected classical approach can provide essentially correct spectral band contours for gas-phase rotational and vibrational-rotational transitions, the cases in which we know accurately the potential energy and dipole moment functions and in which we can compare to accurate quantum calculations, we now turn to higher densities, where our knowledge of the potential energy and dipole functions is less certain, and our ability to compute spectra by alternative means is less developed. We will treat solutions of CO in progressively higher densities of Ar, and finally in liquid Ar.

Various approximation methods,[20] classical, semiclassical and quantum, have been applied to computing vibrational-rotational band contours for diatomics in solution. Examples include the stochastic and diffusional approach of Bratos and co-workers,[17,35] the semiclassical method of Gordon and co-workers,[36-38] and the classical impact study of Koszykowski and Marcus.[20] Our choice to develop a classical (and rather brute-force) molecular dynamic method which includes all degrees of freedom is inspired by our desire to extend the method to more complex solute and solvent molecules and to transient spectra in non-equilibrium systems.

Figures 5 and 6 show experimental band spectra for room temperature CO in different densities of Ar solvent after Coulon *et al*[39] and in liquid Ar at a temperature of 97 °K and a density of 750 amagats (or 2.014×10^{28} atoms m^{-3}) after Buontempo *et al.*[24] (One amagat unit of density is the actual concentration of the particular gas at 0 °C and 1 atm pressure, which would be 2.6869×10^{25} molecules m^{-3} for an ideal gas.)[40] For our theoretical spectra we use the Newtonian classical approach developed above. To reduce edge effects in our dynamics we use minimum image periodic boundary conditions, replicating a truncated octahedron in a space-filling solid tessellation,[10] smoothly reducing our potentials to zero within the radius of the inscribed sphere to avoid discontinuities as atoms cross the boundaries.

The intermolecular potential we use is a simple pairwise Lennard-Jones approximation,

$$V(r) = 4\epsilon\,\{(\sigma/r)^{12} - (\sigma/r)^{6}\}, \tag{37}$$

in which r is the pairwise internuclear distance. For Ar - Ar we use[20] a well-depth $\epsilon=124$ °K k_B (equivalent to 1.712×10^{-21} J) and a zero-crossing radius $\sigma=0.342$ nm. For both Ar - C and Ar - O we use $\epsilon=88$ °K k_B (equivalent to 1.22×10^{-21} J) and $\sigma=0.328$ nm. This Ar - CO potential is a crude fit of two identical two body potentials to the potential surface of Parker and Pack[41] by roughly matching two body potentials to the zero-crossing and well depths for the average of both three body potentials shown in their Fig. 4. The CO intramolecular potential is as before.

In these calculations of CO in Ar, to reduce the computational effort per specific spectrum and allow more ensemble averaging, we use in the molecular dynamics a step size of 10^{-15} s, and then correct the spectra for the $+16$ cm^{-1} shift this produces. Fifty-five atoms of Ar are used in the unit cell. As can be seen in Figs. 5 and 6, the agreement of theory and experiment all the way from the dilute gas phase to the liquid phase is quite satisfactory, given the crudeness of the potential we have used, and the experimental uncertainties.

VI. CONCLUSION

This work shows, at least for the simple system treated, that the combination of classical molecular dynamics, linear response theory, classical ensemble averaging and suitable quantum corrections allows electric dipole rotational and vibrational-rotational band contours to be computed which are in close agreement with quantum calculations and with experimental results. As we have shown, the approach is equally applicable over the range of densities from dilute gas to liquid solution (and it should also apply to solids). We have purposely avoided, at least for now, the additional theoretical complexity[42] inherent in treating the case of strong absorbers in more concentrated solutions, due to the variation of the index of refraction with absorption frequency.

The reason that these classical calculations reproduce so well the observed spectra can be understood as follows. For translational motion, the quantum numbers for the usual effective volumes for atomic motion are large enough that the correspondence principle implies quantum convergence to the classical limit. For rotational motion, the average quantum numbers are moderate, and if one blurs the rotational lines, for example by collisions, the band contours require at most quite small quantum corrections. For vibrational motion, the average quantum numbers are very small, and the correspondence principle limit is far from fulfilled. Thus, at first glance, one is surprised that the classical and quantum agreement is so good. The reason for this agreement is the unique equivalence for quadratic potentials of many averaged measurables for the classical and quantum cases.[43-46] For example, the average energy gain for the forced harmonic oscillator driven by a time varying force $\mathbf{F}(t)$ either from radiation or from collisions is the same classically and quantally, and the quantum expectation values and classical values of position and momentum follow the same classical equations of motion. Thus we find exact agreement between our classical and quantum spectral calculations for harmonic vibrational motion driven by the time varying force from the oscillating electric field of the light, and only the anharmonic part of the potential requires a quantum correction.

We are able to ignore the effects of quantization of the radiation field, in part, because the lifetimes for spontaneous emission are long with respect to other changes in our system once we have introduced collisions. Thus any broadening of our spectra by radiation damping is negligible.

That classical mechanics succeeds so well in reproducing the absorption spectrum does *not* imply that the system would behave classically if it were examined by a different set of measurements. Clearly the vibrational properties are far from classical if one examines, for example, the allowed energies of the system instead of the probability of light absorption versus wavelength or frequency. What *is* implied is that we may *think* about (or compute) the whole system of molecules and internal interactions as well as the interaction of the system with light in a classical manner, applying our well-calibrated and insightful classical intuition, with some confidence that we can arrive at close to the same spectral result as if we had properly handled the real quantal nature of the system. This opens the way to understanding the vibrational spectra of much larger and more complex systems under a wider variety of conditions than is feasible with a quantum approach. We thus believe that the larger difficulties in the computation of vibrational spectral band contours, even for complex molecules and for condensed phases, probably lie on the electronic side of the Born-Oppenheimer separation (potential energy, dipole moment, and polarizability matrix as functions of nuclear position) rather than on the nuclear motion side.

We plan in future papers to show how a parallel approach can be applied to the electric dipole pure rotational and vibrational-rotational spectra of polyatomic molecules as well as to Raman pure rotational and vibrational-rotational spectra, both for gases and condensed phases. In addition, we plan to illustrate the extension of this molecular dynamic and linear response approach to non-equilibrium, time dependent processes, specifically to the computation of transient rotational and vibrational-rotational spectra during the course of chemical change. We believe that the computation and measurement of such spectra can be a promising route to discovering the molecular dynamics of chemical reactions in solution.[3]

ACKNOWLEDGEMENT

We wish to thank the Office of Naval Research, Chemistry, the National Science Foundation, Chemistry, and the National Institutes of Health, Division of Research Resources, for providing the support which has made this work possible. In addition, we wish to thank Philippe Bado, Gary M. White and Steven R. White for their considerable help with the calculations.

APPENDIX: QUANTUM BAND CONTOURS

We will evaluate Eq. (5) quantum mechanically for a diatomic molecule,[47] using rigid-rotor harmonic oscillator transition probabilites, but energies (and thus frequencies and state probabilities) which include anharmonic, centrifugal and vibrational-rotational coupling terms. The transition matrix elements are

$$<f|\mu|i> = <v'J'M'|\mu(R)|vJM>, \tag{A1}$$

in which v is the vibrational, J the total rotational angular momentum and M the z component of angular momentum quantum number for a diatomic molecule with no spin or electronic angular momentum. Primes indicate final state, and we assume integration of the dipole moment operator over electronic coordinates to give $\mu(R)$, the dipole moment as a function of internuclear distance R. By symmetry, $\mu(R)$ must lie along the internuclear axis, so that

$$\mu(R) = \mu(R)\hat{\mathbf{R}}\,, \tag{A2}$$

in which $\hat{\mathbf{R}}$ is a unit vector along the intermolecular axis. Our first approximation is to expand $\mu(R)$ as a Taylor's series, keeping only the first two terms, which gives the standard linear approximation to the dipole moment function

$$\mu(R) \approx \mu_0 + \mu_1 \Delta R \tag{A3}$$

in which $\Delta R = (R - R_e)$ is the deviation from the position R_e at the minimum of the potential curve $V(R)$.

Our second approximation is to evaluate the matrix element in Eq. (A1) using the rigid-rotor harmonic oscillator approximation[47]

$$<v'J'M'|(\mu_0 + \mu_1\Delta R)\hat{\mathbf{R}}|vJM> \approx <v'|(\mu_0 + \mu_1\Delta R)|v><J'M'|\hat{\mathbf{R}}|JM> \tag{A4}$$

$$= \left\{\mu_0\,\delta_{v',v} + \mu_1\delta_{v'-1,v}[(v+1)/2\alpha]^{1/2}\right\}<J'M'|\hat{\mathbf{R}}|JM>\,, \tag{A5}$$

in which δ is the Kronecker delta and $\alpha = m_r\omega_{fi}/\hbar$ (m_r is the reduced mass). Since all M levels have the same energy, we can sum over M in Eq. (5), finding[48,49]

$$\sum_{M=-J}^{J} |<J'M'|\hat{\mathbf{R}}|JM>|^2 = (J+1)\delta_{J'-1,J} + J\delta_{J'+1,J}\,. \tag{A6}$$

We can now insert Eqs. (A5) and (A6) into Eq. (5) and divide the spectrum into a pure rotational absorption spectrum

$$I_R(\omega) = \sum_{v=0}^{\infty}\sum_{J=0}^{\infty} \rho(v,J)\,\mu_0^2\,(J+1)\,\delta\left[\frac{E(v,J+1) - E(v,J)}{\hbar} - \omega\right] \tag{A7}$$

and a vibrational-rotational absorption spectrum, in which the R branch ($J+1 \leftarrow J$) is

$${}^{R}I_{v'}(\omega) = \sum_{v=0}^{\infty}\sum_{J=0}^{\infty} \rho(v,J)\,\mu_1^2\,(J+1)\,[(v+1)/2\alpha]\,\delta\left[\frac{E(v+1,J+1) - E(v,J)}{\hbar} - \omega\right] \tag{A8}$$

and the P branch ($J-1 \leftarrow J$) is

$${}^{P}I_{v'}(\omega) = \sum_{v=0}^{\infty}\sum_{J=1}^{\infty} \rho(v,J)\,\mu_1^2 J\,[(v+1)/2\alpha]\,\delta\left[\frac{E(v+1,J-1) - E(v,J)}{\hbar} - \omega\right] \tag{A9}$$

where in Eqs. (A7-A9)

$$\rho(v,J) = \frac{\exp[-\beta E(v,J)]}{\sum_{v=0}^{\infty}\sum_{J=0}^{\infty}(2J+1)\exp[-\beta E(v,J)]}. \tag{A10}$$

The final approximation is to use energy levels evaluated to second order in perturbation theory, involving the third and fourth derivatives of the potential, giving[47]

$$E(v,J) = h\left[\nu_e(v+\tfrac{1}{2}) + B_e J(J+1) - \nu_e x_e (v+\tfrac{1}{2})^2 - \alpha_e (v+\tfrac{1}{2})J(J+1) - \bar{D}_e J^2(J+1)^2\right] \tag{A11}$$

in which

$$B_e = \frac{\hbar}{4\pi I_e} \tag{A12}$$

$$I_e = m_r R_e^2 \tag{A13}$$

$$\nu_e = (2\pi)^{-1}\left[\frac{V''(R_e)}{m_r}\right]^{1/2} \tag{A14}$$

$$\nu_e x_e = \frac{B_e^2 R_e^4}{4h\nu_e^2}\left[\frac{10B_e R_e^2[V'''(R_e)]^2}{3h\nu_e^2} - V''''(R_e)\right] \tag{A15}$$

$$\alpha_e = \frac{-2B_e^2}{\nu_e}\left[\frac{2B_e R_e^3 V'''(R_e)}{h\nu_e^2} + 3\right] \tag{A16}$$

and

$$\bar{D}_e = \frac{4B_e^3}{\nu_e^2}. \tag{A17}$$

In the above, $V''(R_e)$, $V'''(R_e)$ and $V''''(R_e)$ are the second, third and fourth derivatives of the internuclear potential at the potential minimum.

All three of the above approximations (linearity of the dipole moment function, rigid rotor - harmonic oscillator evaluation of the transition matrix-elements, and energy level evaluation by second order perturbation theory through third and fourth derivatives of the potential function) may be extended to higher terms to give higher accuracy,[33,50-54] but in the example treated here it is unwarranted.

Using these formulas, we can evaluate the quantum spectrum, and then obtain the band contours by broadening the δ functions, for example, into Gaussians

$$\delta(\omega_{fi}-\omega) \rightarrow (\gamma/\pi)^{1/2}\exp[\gamma(\omega_{fi}-\omega)^2] \tag{A18}$$

and letting γ decrease until the individual rotational peaks merge.

By evaluating Eqs. (A7-A9) at successively lower values of Planck's constant, until the resulting functions converge to a limit, we can compute the correspondence principle classical $I^C(\omega)$, and through applying the same technique to Eq. (2) we compute the correspondence principle classical spectrum, $\alpha^C(\omega)$.

References

1. K. R. Wilson, in *Minicomputers and Large Scale Computations*, edited by P. Lykos (American Chemical Society, Washington, 1977).
2. K. R. Wilson, in *Computer Networking and Chemistry*, edited by P. Lykos (American Chemical Society, Washington, 1975).
3. P. H. Berens and K. R. Wilson, in *Picosecond Phenomena II*, edited by R. Hochstrasser, W. Kaiser, and C. V. Shank (Springer-Verlag, Berlin, 1980).
4. R. G. Gordon, *Advan. Magn. Reson.* **3**, 1 (1968).
5. B. J. Berne, in *Physical Chemistry, An Advanced Treatise*, edited by D. Henderson (Academic Press, New York, 1971) Vol. VIIIB, Chap. 9.
6. D. A. McQuarrie, *Statistical Mechanics* (Harper and Row, New York, 1976) pp. 467-592.
7. D. W. Noid, M. L. Koszykowski, and R. A. Marcus, *J. Chem. Phys.* **67**, 404 (1977).
8. D. Beeman, *J. Comput. Phys.* **20**, 130 (1976).
9. H. C. Andersen, (Private Communication), 1980.
10. D. J. Adams, in *The Problem of Long-Range Forces in the Computer Simulation of Condensed Media*, edited by D. Ceperely (National Resource for Computation in Chemistry, Berkeley, 1980) p. 13.
11. E. O. Brigham, *The Fast Fourier Transform* (Prentice-Hall, Englewood Cliffs, 1974).
12. R. P. Futrelle and D. J. McGinty, *Chem. Phys. Lett.* **12**, 285 (1971).
13. F. J. Harris, *Proc. IEEE* **66**, 51 (1978).
14. P. Schofield, *Phys. Rev. Lett.* **4**, 39 (1960).
15. B. J. Berne, J. Jortner, and R. Gordon, *J. Chem. Phys.* **47**, 1600 (1967).
16. G. A. Korn and T. M. Korn, *Mathematical Handbook for Scientists and Engineers* (McGraw-Hill, New York, 1961) pp. 742-743.
17. S. Bratoz, J. Rios, and Y. Guissani, *J. Chem. Phys.* **52**, 439 (1970).
18. D. Steele, *Theory of Vibrational Spectroscopy* (W. B. Saunders, Philadelphia, 1971) p. 124.
19. G. Levi, J. P. Marsault, F. Marsualt-Herail, and R. E. D. McClung, *J. Chem. Phys.* **63**, 3543 (1975).
20. M. L. Koszykowski and R. A. Marcus, *J. Chem. Phys.* **63**, 1216 (1978).
21. K. P. Huber and G. Herzberg, *Molecular Spectra and Molecular Structure IV. Constants of Diatomic Molecules* (Van Nostrand Reinhold, New York, 1979).
22. J. N. Huffaker, *J. Chem. Phys.* **64**, 3175 and 4564 (1976).
23. J. N. Huffaker, *J. Mol. Spectrosc.* **65**, 1 (1977).
24. U. Buontempo, S. Cunsolo, and G. Jacucci, *J. Chem. Phys.* **59**, 3750 (1973).
25. D. H. Rank, G. Skorinko, D. P. Eastman, and T. A. Wiggins, *J. Mol. Spectrosc.* **4**, 518 (1960).
26. R. L. Armstrong and H. L. Welsh, *Canad. J. Phys.* **43**, 547 (1965).
27. J. P. Bouanich, *J. Quant. Spectrosc. Radiat. Transfer* **16**, 1119 (1976).
28. R. A. Toth, R. H. Hunt, and E. K. Plyler, *J. Mol. Spectrosc.* **32**, 85 (1969).
29. J. S. Muenter, *J. Mol. Spectrosc.* **55**, 490 (1975).
30. C. Chackerian, Jr., *J. Chem. Phys.* **65**, 4228 (1976).
31. S. M. Kirschner, R. J. LeRoy, J. F. Ogilvie, and R. H. Tipping, *J. Mol. Spectrosc.* **65**, 306 (1977).

32. K. Kirby-Docken and B. Liu, *J. Chem. Phys.* **66**, 4309 (1977).
33. R. A. Toth, R. H. Hunt, and E. K. Plyler, *J. Mol. Spectrosc.* **32**, 74 (1969).
34. L. A. Pugh and K. N. Rao, in *Molecular Spectroscopy: Modern Research*, edited by K. N. Rao (Academic Press, New York, 1976) Vol. II, pp. 165-227.
35. J. C. Leicknam, Y. Guissani, and S. Bratos, *J. Chem. Phys.* **68**, 3390 (1978).
36. R. G. Gordon and R. P. McGinnis, *J. Chem. Phys.* **49**, 2455 (1968).
37. R. G. Gordon and R. P. McGinnis, *J. Chem. Phys.* **55**, 4898 (1971).
38. W. B. Neilsen and R. G. Gordon, *J. Chem. Phys.* **58**, 4131 and 4149 (1973).
39. R. Coulon, L. Galatry, B. Okseengorn, S. Rubin, and B. Vodar, *J. Physique Rad.* **15**, 641 (1954).
40. A. S. Friedman, in *American Institute of Physics Handbook*, edited by D. E. Gray (McGraw-Hill, New York, 1963) pp. 4-158.
41. G. A. Parker and R. T. Pack, *J. Chem. Phys.* **69**, 3268 (1978).
42. R. L. Fulton, *J. Chem. Phys.* **55**, 1386 (1971).
43. K. Gottfried, *Quantum Mechanics, Vol. I, Fundamentals* (W. A. Benjamin, New York, 1966) pp. 66-74, 256-264.
44. K. E. Holdy, L. C. Klotz, and K. R. Wilson, *J. Chem. Phys.* **52**, 4588 (1970).
45. F. E. Heidrich, K. R. Wilson, and D. Rapp, *J. Chem. Phys.* **54**, 3885 (1971).
46. E. J. Heller, *J. Chem. Phys.* **62**, 1544 (1975).
47. I. R. Levine, *Molecular Spectroscopy* (John Wiley and Sons, New York, 1975) pp. 142-194.
48. H. C. Allen, Jr. and P. C. Cross, *Molecular Vib-Rotors* (John Wiley, New York, 1963).
49. J. E. Wollrab, *Rotational Spectra and Molecular Structure* (Academic Press, New York, 1967) p. 44.
50. H. S. Heaps and G. Herzberg, *Z. Physik* **133**, 48 (1952).
51. R. Herman and R. F. Wallis, *J. Chem. Phys.* **23**, 637 (1955).
52. R. Herman and R. J. Rubin, *Astrophys. J.* **121**, 533 (1955).
53. R. Herman, R. W. Rothery, and R. J. Rubin, *J. Mol. Spectrosc.* **2**, 269 (1958).
54. R. M. Herman, R. H. Tipping, and S. Short, *J. Chem. Phys.* **53**, 595 (1970).

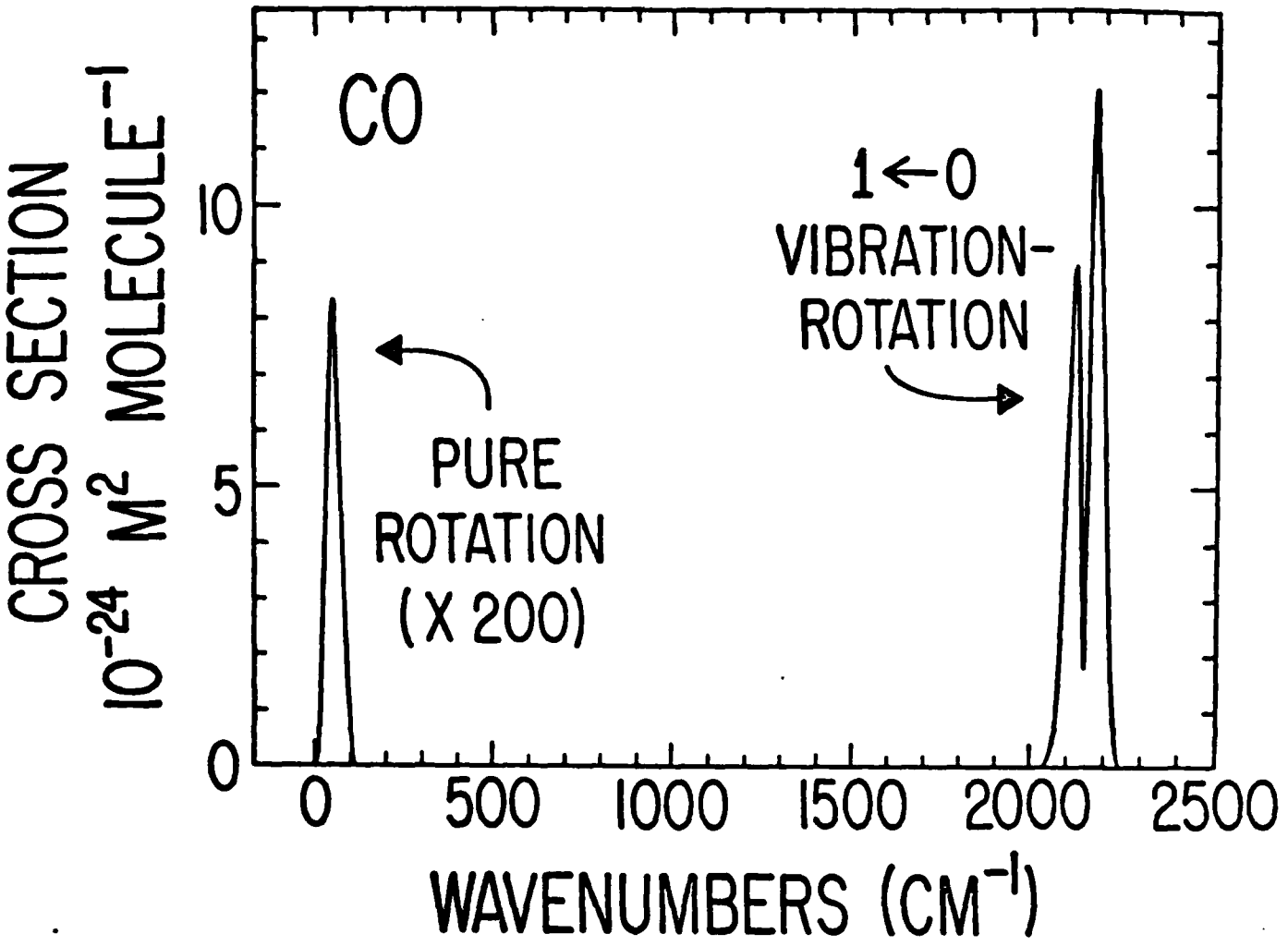

Figure 1. Absorption spectrum for gas phase CO at 298 °K, showing pure rotational band contour on left and fundamental vibrational-rotational band contour on the right. Subsequent figures examine each of these bands in detail.

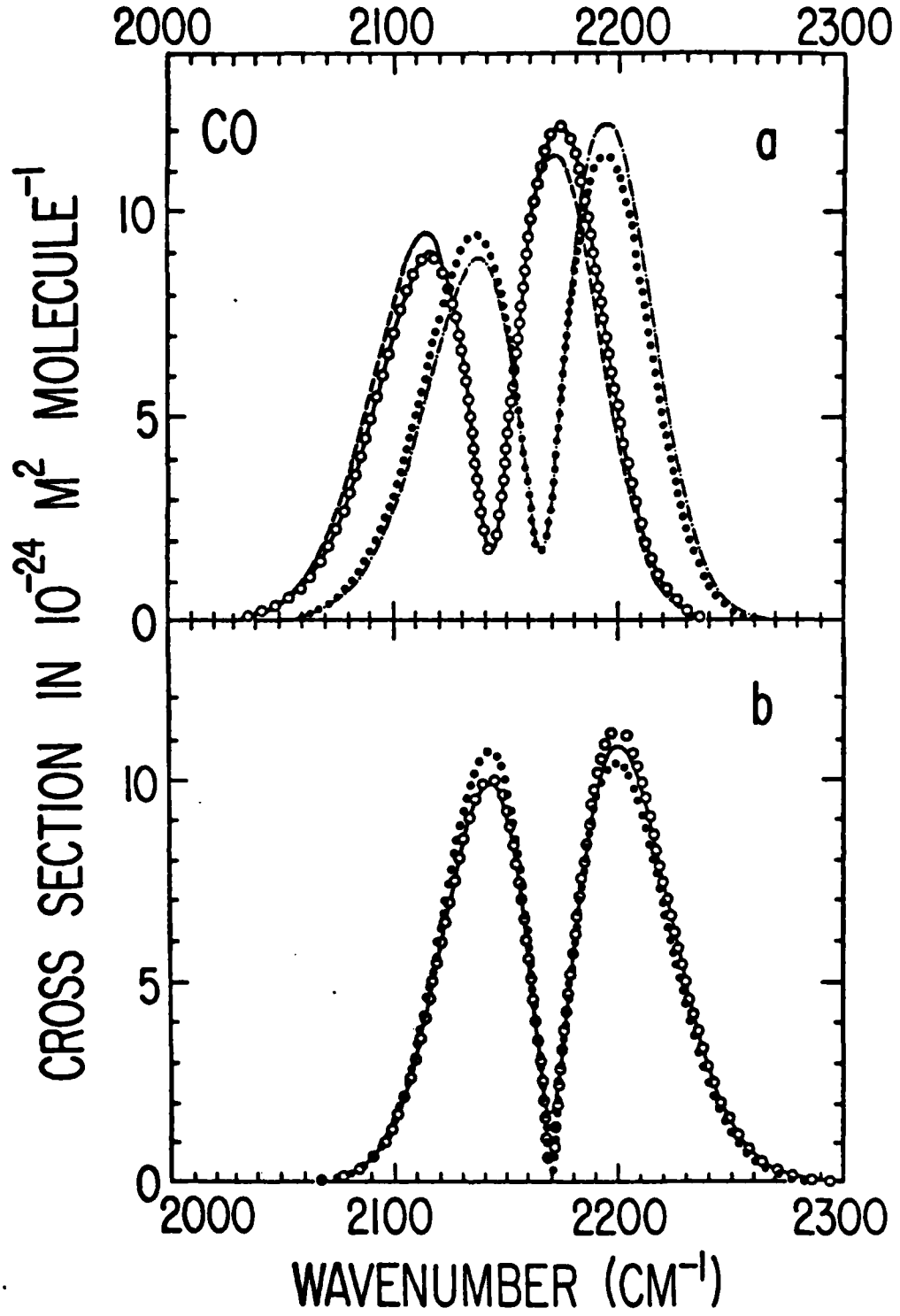

Figure 2. Quantum corrections to classical vibrational-rotational spectra. In the upper panel, for the real anharmonic potential for CO, the solid line (under the open circles) shows the actual quantum band contour for gas phase CO. The dotted line shows the correspondence limit classical band. The dashed line shows the effect of applying the vibrational anharmonic offset quantum correction alone to the classical band. The dashed and dotted line shows the effect of applying the rotational detailed balance quantum correction alone. The open circles show the effect of applying both corrections together. In the lower panel, similar contours are shown for CO as a harmonic oscillator, keeping the same second derivative at the equilibrium internuclear distance as for the real CO potential. There is now no anharmonic offset quantum correction. Note the large increase in the asymmetry between the maximum intensities of the P and R branches produced by the anharmonicity in the potential.

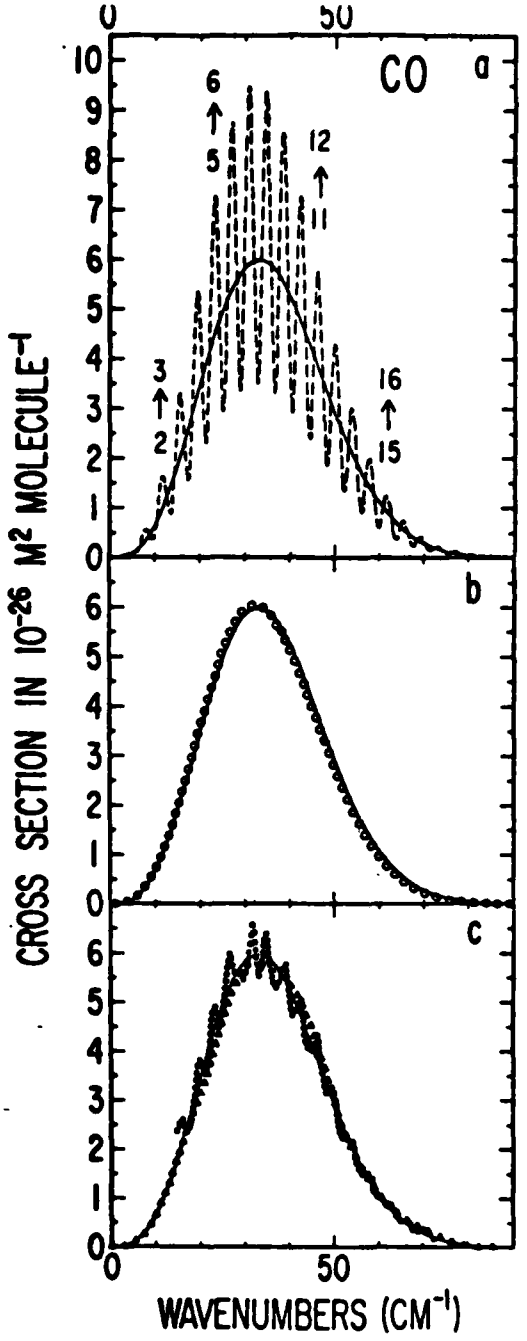

Figure 3. Pure rotational spectrum for gas phase CO at 129°K. The upper panel shows as a dashed line the quantum rotational lines, (partially broadened by Eq. (A18) for illustration) and as a solid line the quantum rotational band contour from further broadening the individual rotational lines until they fuse into a smooth contour. The middle panel shows again the quantum band contour as a solid line and the classical $\hbar \to 0$ limit correspondence principle contour as open circles which fall very close to the quantum contour. The lower panel shows the quantum contour as a solid line and the Newtonian classical (classical molecular dynamics, classical linear response, classical statistical mechanical ensemble average) band as triangles. The Newtonian spectra are an average over an ensemble of 10,000 single-molecule time histories of 24.6×10^{-12}s each with 10^{-16}s integration steps, run in groups of 300 non-interacting molecules. The dotted line is the experimental gas phase spectrum of Buontempo *et al*, with Ar added to partially broaden the rotational lines. We have multiplied their experimental cross sections by a scaling factor of 1.15, which may well be within their experimental error, to better match both our calculations and the sum rule of Eq. (36) which they cite, both of which are based on the accepted values of the average permanent dipole moment of CO.

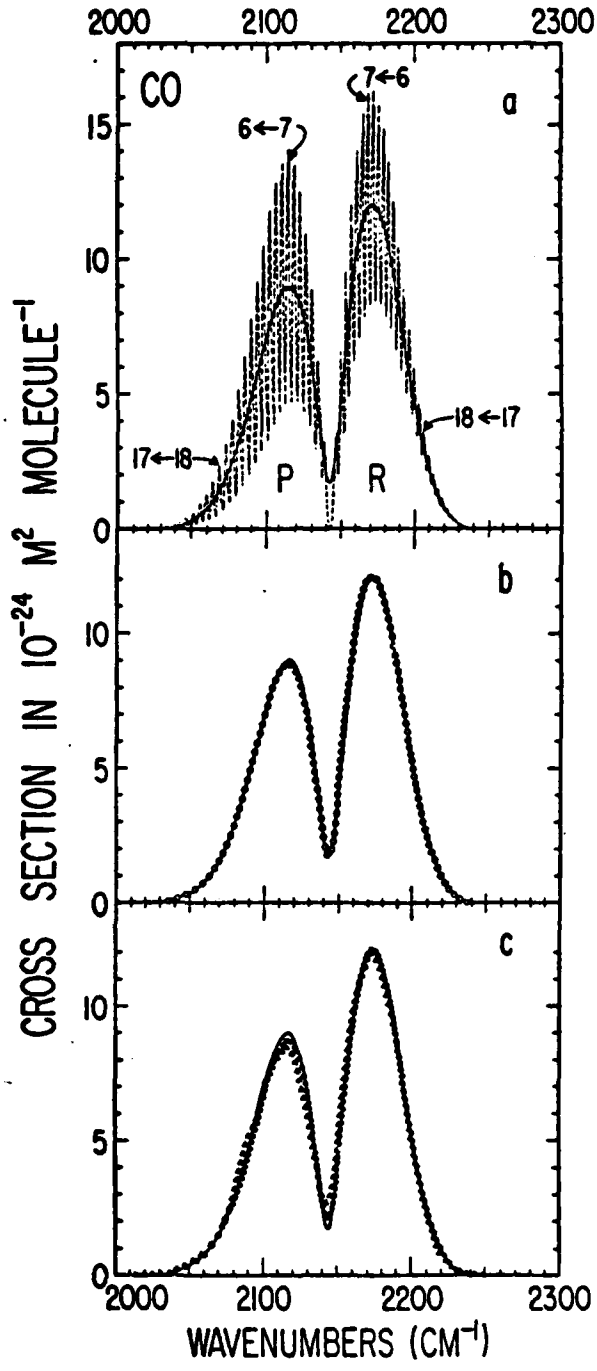

Figure 4. Vibrational-rotational fundamental band spectrum for gas phase CO at 298 °K. The upper panel shows as a dashed line the quantum vibrational-rotational lines (partially broadened by Eq. (A18) for illustration), and as a solid line the quantum rotational band contour from broadening the individual vibrational-rotational lines further until they fuse into a smooth contour. The middle panel shows again the quantum band contour as a solid line and the quantum corrected classical $\hbar \to 0$ limit correspondence principle band as open circles which match very closely the quantum contour. The lower panel shows the quantum contour as a solid line and the quantum-corrected Newtonian classical (classical molecular dynamics, classical linear response, classical statistical mechanical ensemble average) band as triangles. The Newtonian spectra are averaged over an ensemble of 10,000 single-molecule time histories of 24.6×10^{-12}s each with a 10^{-16}s integration step, the dynamics run in groups of 300 non-interacting molecules. The dotted line is the experimental gas phase spectrum of Armstrong and Welsh with He added to broaden the individual lines, which was given with no absolute intensity units, and is thus scaled to match the theoretical curves.

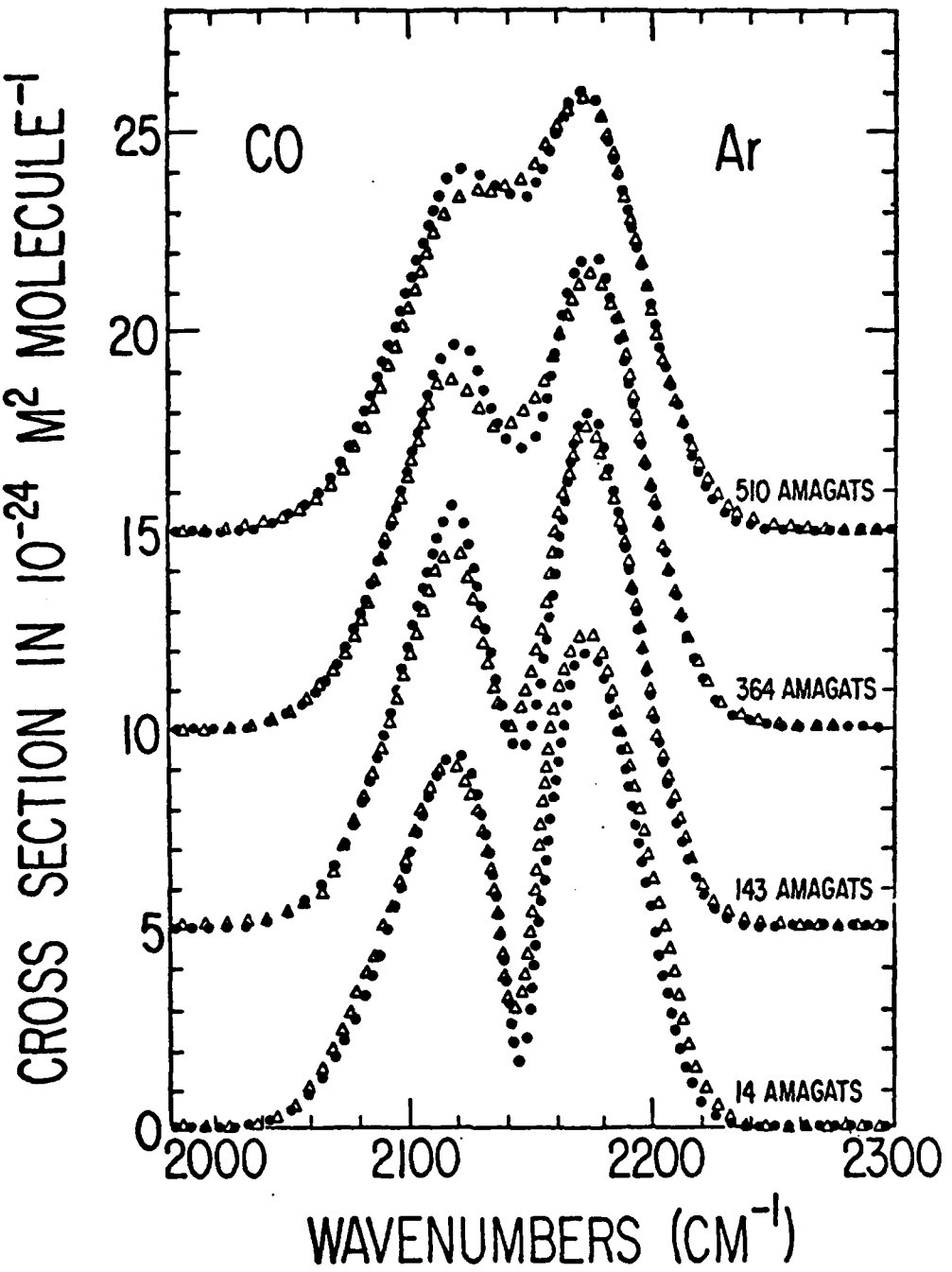

Figure 5. Vibrational-rotational infrared fundamental band for CO in increasing densities of Ar. The triangles show the theoretical spectra for solutions of CO in various densities of gas phase Ar as computed from "Newtonian" theory (molecular dynamics, linear response, statistical mechanics all carried out classically and then quantum corrected). Each spectrum is averaged over an ensemble of 500 runs of 24.6×10^{-12}s in length, with a 10^{-15}s step size using periodic boundary conditions. The calculation of the dynamics for each run took 12 minutes of real time. 55 Ar atoms and 1 CO are used, except for the 14 amagat computation which is 1400 runs with 17 Ar atoms. *The dotted line shows the corresponding experimental spectra from* Coulon *et al* for gas-phase solutions of CO in Ar at room temperature. All the experimental cross-sections are scaled by a factor of 0.82, which is perhaps within their experimental uncertainty, and is certainly within the range of other historical experimental intensity measurements for the CO fundamental intensity, in order to more closely match the theoretical calculations, which are based on more recent dipole derivative measurements. In all cases, the index of refraction, n, in the linear response equations is set to 1.0.

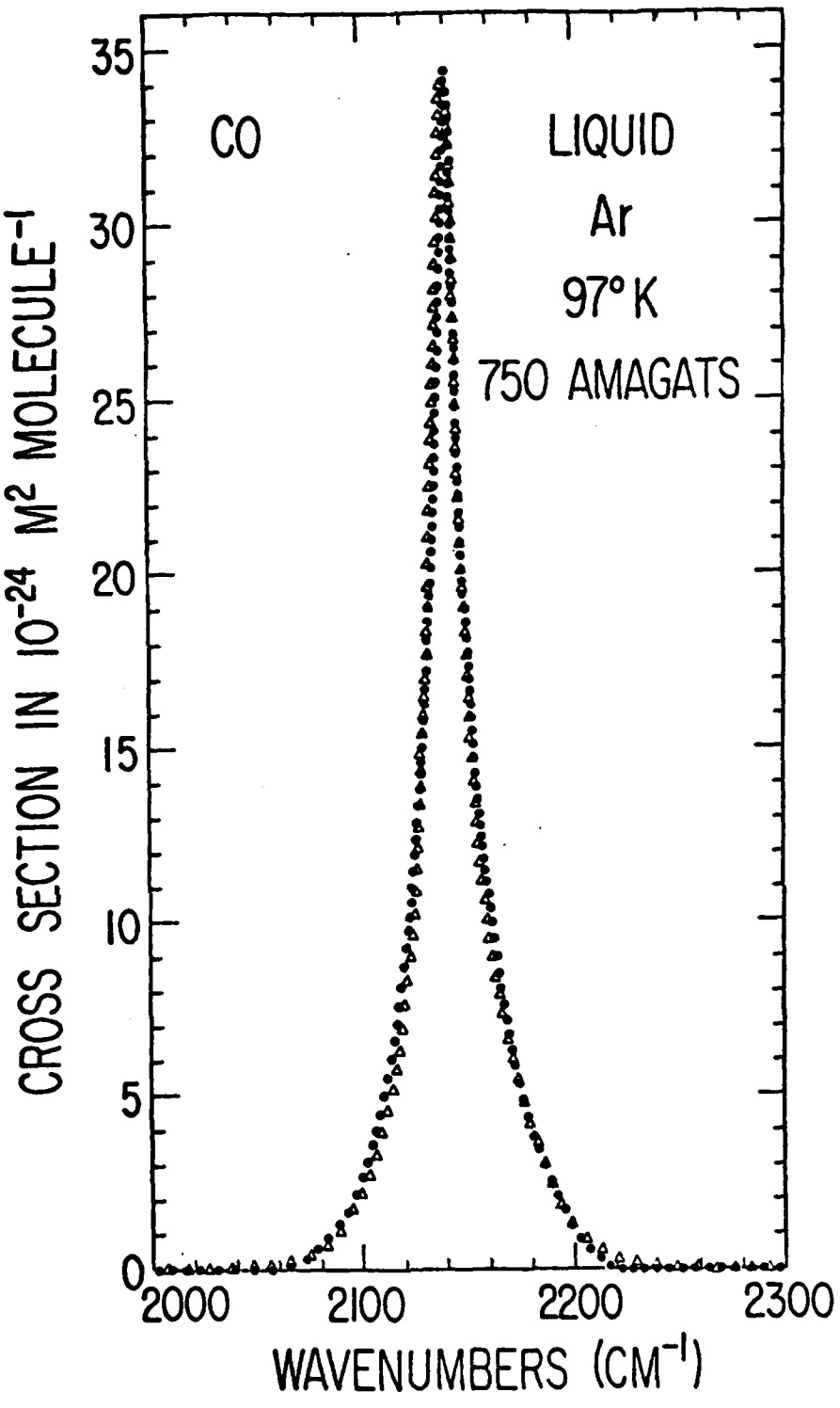

Figure 6. CO in liquid Ar plotted to the same scale as Fig. 5. Open triangles are the "Newtonian" theoretical calculations, for 55 Ar atoms and one CO using periodic boundary conditions. The spectra are averaged over 500 runs of 24.6×10^{-12}s each with a 10^{-15}s step size at 97°K. The dotted line shows the liquid phase experimental measurement of Buontempo *et al* which is given with no absolute units, and is thus scaled to match the theoretical calculations. It is approximately corrected for the indicated instrumental resolution. The anharmonic shift computed from Eq. (35) is -25 cm^{-1} at 97°K, which is not quite sufficient to match the experimental liquid phase data, so we have added an additional -5 cm^{-1} solvent shift (approximately a frequency scale factor of 0.998) to our computed data to match the experimental measurement. The index of refraction, n, in the linear response equations is set to 1.0.

TECHNICAL REPORT DISTRIBUTION LIST, GEN

	No. Copies
Office of Naval Research Attn: Code 472 800 North Quincy Street Arlington, Virginia 22217	2
ONR Branch Office Attn: Dr. George Sandoz 536 S. Clark Street Chicago, Illinois 60605	1
ONR Area Office Attn: Scientific Dept. 715 Broadway New York, New York 10003	1
ONR Western Regional Office 1030 East Green Street Pasadena, California 91106	1
ONR Eastern/Central Regional Office Attn: Dr. L. H. Peebles Building 114, Section D 666 Summer Street Boston, Massachusetts 02210	1
Director, Naval Research Laboratory Attn: Code 6100 Washington, D.C. 20390	1
The Assistant Secretary of the Navy (RE&S) Department of the Navy Room 4E736, Pentagon Washington, D.C. 20350	1
Commander, Naval Air Systems Command Attn: Code 310C (H. Rosenwasser) Department of the Navy Washington, D.C. 20360	1
Defense Technical Information Center Building 5, Cameron Station Alexandria, Virginia 22314	12
Dr. Fred Saalfeld Chemistry Division, Code 6100 Naval Research Laboratory Washington, D.C. 20375	1
U.S. Army Research Office Attn: CRD-AA-IP P.O. Box 1211 Research Triangle Park, N.C. 27709	1
Naval Ocean Systems Center Attn: Mr. Joe McCartney San Diego, California 92152	1
Naval Weapons Center Attn: Dr. A. B. Amster, Chemistry Division China Lake, California 93555	1
Naval Civil Engineering Laboratory Attn: Dr. R. W. Drisko Port Hueneme, California 93401	1
Department of Physics & Chemistry Naval Postgraduate School Monterey, California 93940	1
Dr. A. L. Slafkosky Scientific Advisor Commandant of the Marine Corps (Code RD-1) Washington, D.C. 20380	1
Office of Naval Research Attn: Dr. Richard S. Miller 800 N. Quincy Street Arlington, Virginia 22217	1
Naval Ship Research and Development Center Attn: Dr. G. Bosmajian, Applied Chemistry Division Annapolis, Maryland 21401	1
Naval Ocean Systems Center Attn: Dr. S. Yamamoto, Marine Sciences Division San Diego, California 91232	1
Mr. John Boyle Materials Branch Naval Ship Engineering Center Philadelphia, Pennsylvania 19112	1

TECHNICAL REPORT DISTRIBUTION LIST, GEN

	No. Copies
Dr. Rudolph J. Marcus Office of Naval Research Scientific Liaison Group American Embassy APO San Francisco 96503	1
Mr. James Kelley DTNSRDC Code 2803 Annapolis, Maryland 21402	1

TECHNICAL REPORT DISTRIBUTION LIST, 051B

	No. Copies
Professor K. Wilson Department of Chemistry, B-014 University of California, San Diego La Jolla, California 92093	1
Professor C. A. Angell Department of Chemistry Purdue University West Lafayette, Indiana 47907	1
Professor P. Meijer Department of Physics Catholic University of America Washington, D.C. 20064	1
Dr. S. Greer Chemistry Department University of Maryland College Park, Maryland 20742	1
Professor P. Delahay New York University 100 Washington Square East New York, New York 10003	1
Dr. T. Ashworth Department of Physics South Dakota School of Mines & Technology Rapid City, South Dakota 57701	1
Dr. G. Gross New Mexico Institute of Mining & Technology Socorro, New Mexico 87801	1
Dr. J. Kassner Space Science Research Center University of Missouri - Rolla Rolla, Missouri 65401	1
Dr. J. Telford University of Nevada System Desert Research Institute Lab of Atmospheric Physics Reno, Nevada 89507	1
Dr. B. Vonnegut State University of New York Earth Sciences Building 1400 Washington Avenue Albany, New York 12203	1
Dr. Hank Loos Laguna Research Laboratory 21421 Stans Lane Laguna Beach, California 92651	1
Dr. John Latham University of Manchester Institute of Science & Technology P.O. Box 88 Manchester, England M601QD	1

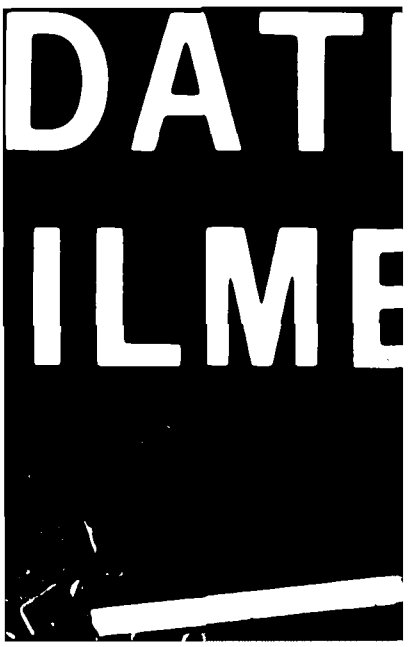
DAT
ILME